The Arabidopsis Ortholog of Rice DWARF27 Acts Upstream of MAX1 in the Control of Plant Development by Strigolactones[1][C][W][OA]

Mark T. Waters, Philip B. Brewer, John D. Bussell, Steven M. Smith, and Christine A. Beveridge*

Plant Energy Biology (M.T.W., J.D.B., S.M.S.) and School of Chemistry and Biochemistry (S.M.S.), University of Western Australia, Crawley, Western Australia 6009, Australia; and School of Biological Sciences, University of Queensland, St Lucia, Queensland 4072, Australia (P.B.B., C.A.B.)

Strigolactones (SLs) are carotenoid-derived plant hormones that regulate shoot branching, secondary growth, root development, and responses to soil phosphate. In Arabidopsis (*Arabidopsis thaliana*), SL biosynthesis requires the sequential action of two carotenoid cleavage dioxygenases, MORE AXILLARY GROWTH3 (MAX3) and MAX4, followed by a cytochrome P450, MAX1. In rice (*Oryza sativa*), the plastid-localized protein DWARF27 (OsD27) is also necessary for SL biosynthesis, but the equivalent gene in Arabidopsis has not been identified. Here, we use phylogenetic analysis of D27-like sequences from photosynthetic organisms to identify AtD27, the likely Arabidopsis ortholog of OsD27. Using reverse genetics, we show that AtD27 is required for the inhibition of secondary bud outgrowth and that exogenous application of the synthetic SL GR24 can rescue the increased branching phenotype of an *Atd27* mutant. Furthermore, we use grafting to demonstrate that AtD27 operates on a nonmobile precursor upstream of MAX1 in the SL biosynthesis pathway. Consistent with the plastid localization of OsD27, we also show that AtD27 possesses a functional plastid transit peptide. We demonstrate that *AtD27* transcripts are subject to both local feedback and auxin-dependent signals, albeit to a lesser extent than *MAX3* and *MAX4*, suggesting that early steps in SL biosynthesis are coregulated at the transcriptional level. By identifying an additional component of the canonical SL biosynthesis pathway in Arabidopsis, we provide a new tool to investigate the regulation of shoot branching and other SL-dependent developmental processes.

Strigolactones (SLs) are a relatively new class of plant hormones that control multiple facets of plant growth and development. SLs were originally identified from root exudates as organic compounds that stimulated the germination of particular parasitic weeds (Cook et al., 1966; Xie et al., 2010) and were more recently found to promote the symbiosis between plants and mycorrhizal fungi (Akiyama et al., 2005; Dor et al., 2011). The most widely characterized role of SL in plant development is in the inhibition of shoot branching (Dun et al., 2009a; Domagalska and Leyser, 2011). In addition to enhanced shoot branching, SL-deficient and SL response mutants also exhibit reduced stature, suppressed development of the cambium ring in the main stem (secondary growth), and enhanced lateral and adventitious root development (Stirnberg et al., 2002; Arite et al., 2007; Agusti et al., 2011; Kapulnik et al., 2011; Rasmussen et al., 2012). It is also likely that SLs form part of the signaling system used for responding to available soil nutrients. In wild-type plants, SL content is greatly enhanced under phosphate deficiency, which promotes lateral root and root hair lengthening and mycorrhizal associations, while suppressing aerial growth via reduced shoot branching (Umehara et al., 2010; Kapulnik et al., 2011; Kohlen et al., 2011; Ruyter-Spira et al., 2011).

SLs are carotenoid-derived terpenoid lactones. Only four enzymes have been attributed to this biosynthetic pathway, and only three of these have been described in Arabidopsis (*Arabidopsis thaliana*; Xie et al., 2010). These are encoded by the *MORE AXILLARY GROWTH* genes *MAX1*, *MAX3*, and *MAX4*. MAX3 and MAX4 are carotenoid cleavage dioxygenases (CCD7 and CCD8, respectively) that act in the chloroplast to cleave a carotenoid substrate. MAX1, a cytochrome P450, acts downstream on a mobile intermediate that can traverse a graft union. In Arabidopsis, *MAX3* and *MAX4* are largely expressed in the vasculature and function in the shoot and root. *MAX3* and *MAX4* transcripts are regulated both by auxin and by long- and short-distance feedback systems that depend on SL signaling and

[1] This work was supported by the Australian Research Council (grant nos. DP1096717 to S.M.S. and DP110100997 to C.A.B.) and by a University of Western Australia-University of Queensland Bilateral Research Collaboration award (to S.M.S. and C.A.B.).

* Corresponding author; e-mail c.beveridge@uq.edu.au.

The author responsible for distribution of materials integral to the findings presented in this article in accordance with the policy described in the Instructions for Authors (www.plantphysiol.org) is: Christine A. Beveridge (c.beveridge@uq.edu.au).

[C] Some figures in this article are displayed in color online but in black and white in the print edition.

[W] The online version of this article contains Web-only data.

[OA] Open Access articles can be viewed online without a subscription.

www.plantphysiol.org/cgi/doi/10.1104/pp.112.196253

response (Bennett et al., 2006; Brewer et al., 2009; Hayward et al., 2009). Based on impaired SL response in corresponding mutants of Arabidopsis and rice (*Oryza sativa*), two proteins have been identified as necessary for this process: the F-box protein AtMAX2/OsD3 (Gomez-Roldan et al., 2008; Umehara et al., 2008) and the α/β-fold hydrolase family protein AtD14/OsD14 (Arite et al., 2009; Waters et al., 2012). Relative to wild-type plants, the SL response mutants produce elevated amounts of SL, presumably due to impaired feedback on SL biosynthesis (Umehara et al., 2008; Arite et al., 2009; Kohlen et al., 2011). Accordingly, *MAX3* and *MAX4* gene expression is greatly enhanced in *max2* mutants (Hayward et al., 2009).

In rice, a plastid-targeted protein, DWARF27 (D27), is required for SL biosynthesis (Lin et al., 2009). As with other SL mutants in rice, the *d27* mutant has a highly tillered and dwarf habit, although the phenotype of *d27* is intermediate between the wild type and other characterized SL-related mutants. Like *MAX3* and *MAX4* SL biosynthesis genes, *D27* is expressed in the vasculature. *D27* also has strong expression in axillary buds (Lin et al., 2009). Recent in vitro evidence suggests that D27 is a β-carotene isomerase that converts all-trans-β-carotene into 9-cis-β-carotene, which is then further processed by CCD7 and CCD8 into a SL precursor termed carlactone (Alder et al., 2012). If this biochemical activity is also the case in planta, it is likely that D27 acts upstream of MAX1 in the control of the biosynthesis of a mobile shoot-branching signal. The availability of an equivalent *d27* mutant in a species amenable to grafting would allow a more direct test of this hypothesis. Moreover, it will allow an extended genetic, biochemical, and physiological analysis of SL biosynthesis and its regulation. In this study, we identify the Arabidopsis ortholog of *OsD27* and characterize it with respect to its SL response, expression profile, and regulation and use grafting to place it within the SL biosynthesis pathway.

RESULTS

At1g03055 Is Orthologous to *OsD27*

The Arabidopsis genome encodes three proteins with superficial similarity to rice OsD27. To identify the likely ortholog of OsD27, we performed a phylogenetic analysis of D27-like proteins from land plants, green algae, and cyanobacteria. The eukaryotic sequences broadly grouped into three distinct clades, two of which (clades 1 and 2) only contained representatives from land plants, while the third (clade 3) also contained members from chlorophyte algae and diatoms (Fig. 1). With three cyanobacterial proteins serving as an outgroup, the phylogeny suggests that there was a single D27-like gene copy in the common ancestor of the chlorophyte algae and the land plants. Subsequently, the first of two gene duplication events took place in the lineage leading to the land plants, giving rise to clades 1 and 2. The long branches within clade 3, indicative of long periods of sequence divergence, further suggest that this group of proteins arose prior to, and is functionally distinct from, clades 1 and 2. Intriguingly, several gene duplication events have occurred independently within the individual algal lineages, leading to extensive paralogy within clade 3.

The clades specific to land plants, clades 1 and 2, both had strong Bayesian posterior support, and the two groups together formed a superclade that was also strongly supported. Clades 1 and 2 each contained a representative sequence from the moss *Physcomitrella patens*, indicating that each group derived from a second gene duplication event that occurred during the early evolution of the land plants. Clade 1 contained OsD27, its ortholog in *Medicago truncatula* (Liu et al., 2011), and an Arabidopsis protein encoded by *At1g03055*. Notably, two other Arabidopsis proteins with similarity to OsD27, encoded by *At1g64680* and *At4g01995*, unambiguously were assigned to clades 2 and 3, respectively. Thus, we concluded that *At1g03055* is the likely Arabidopsis ortholog of *OsD27*. Nevertheless, the presence of other D27-like proteins in land plant genomes is indicative of potential genetic redundancy.

The *AtD27* transcript comprises seven exons, and the exon length and structure are highly conserved with the *MtD27* and *OsD27* mRNAs, further supporting orthology between the three genes (Fig. 1B). The AtD27 protein is predicted to be 264 amino acids long and shares 48% pairwise identity with OsD27 (excluding the predicted plastid transit peptides; Supplemental Fig. S1). At present, the D27 protein family does not possess any annotated InterPro domains and belongs to a "domain of unknown function" family (Pfam: DUF4033) of 91 eukaryotic and eubacterial sequences, which are widely represented in Figure 1A. However, the rice D27 protein binds a nonheme iron cofactor, which presumably is required for redox-based activity as a β-carotene isomerase (Lin et al., 2009; Alder et al., 2012).

AtD27 Is Required for the Regulation of Axillary Branching

A search of available germplasm collections for mutations in *AtD27* revealed three possible T-DNA insertion alleles among the GABI-Kat collection (Kleinboelting et al., 2012). Of these, two were confirmed to carry a T-DNA insertion within the *At1g03055* locus. A T-DNA copy resides within the fifth exon in GK-134E08 and in the seventh exon in GK-774D06 (Fig. 2A). Reverse transcription (RT)-PCR analysis showed that both alleles result in the accumulation of incomplete *AtD27* transcripts, consistent with the predicted T-DNA location (Fig. 2B). However, only one of these two alleles resulted in a clear mutant phenotype: in plants homozygous for the GK-134E08 insertion, adult plants exhibited a substantial increase in axillary rosette branches relative to wild-type controls, while GK-

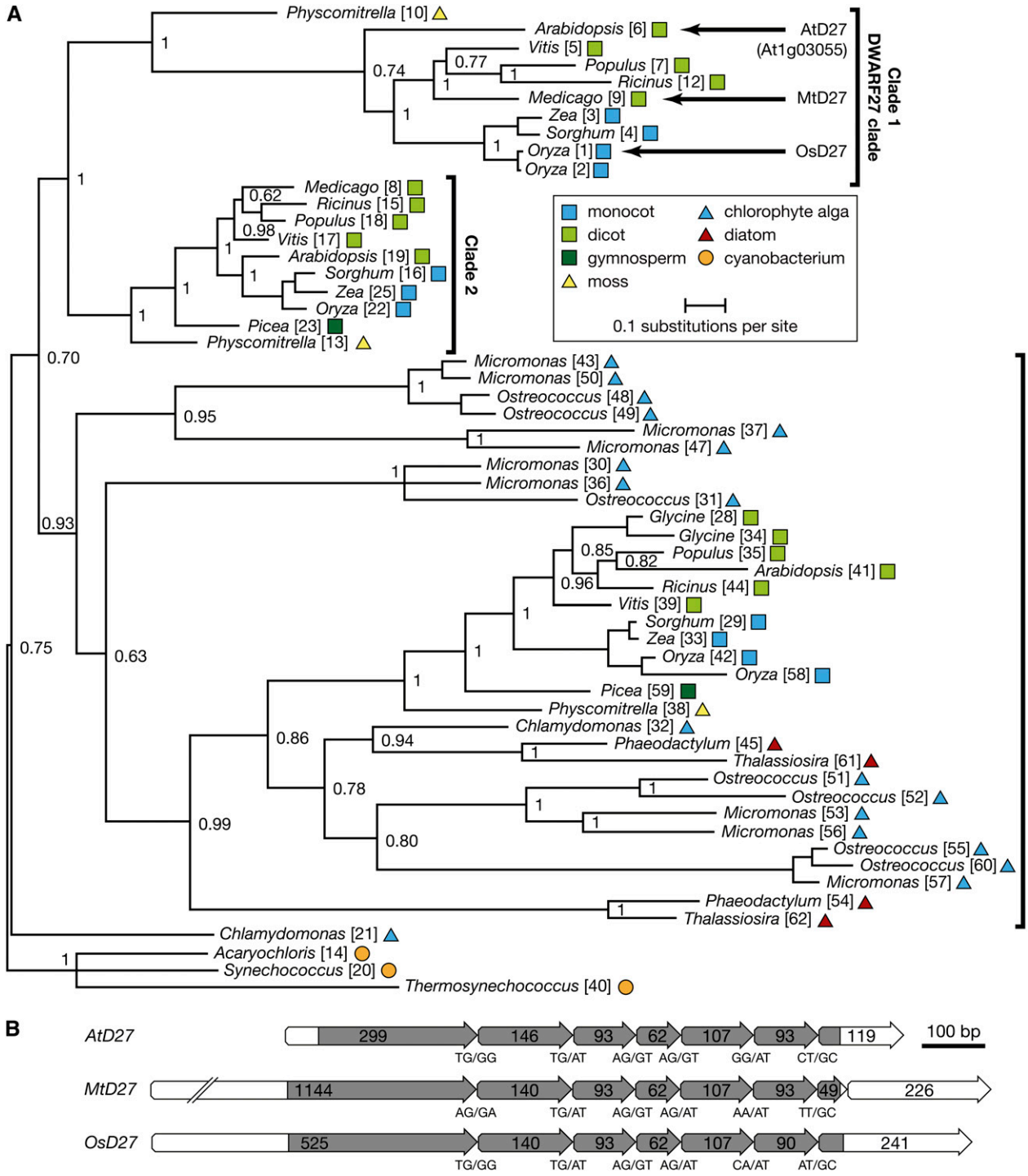

Figure 1. *At1g03055* encodes the Arabidopsis ortholog of rice D27. A, Bayesian inference phylogeny produced from an alignment of D27-like protein sequences from land plants, green algae, and cyanobacteria. Topology support for nodes is given by posterior probability. Terminals are labeled with the genus name followed by a sequence identifier, as detailed in Supplemental Table S2. The tree is rooted on the cyanobacterial clade, based on their ancestral relationship to chloroplasts in photosynthetic eukaryotes. B, Exon structure of *AtD27*, *MtD27*, and *OsD27* mRNAs. A block arrow denotes each exon. Numbers indicate the length of each exon in bp. Protein-coding sequences are indicated by gray fill, and white fill denotes noncoding untranslated regions. The two nucleotides on either side of each exon-exon interface are indicated, with splice junctions denoted by a forward slash (/). [See online article for color version of this figure.]

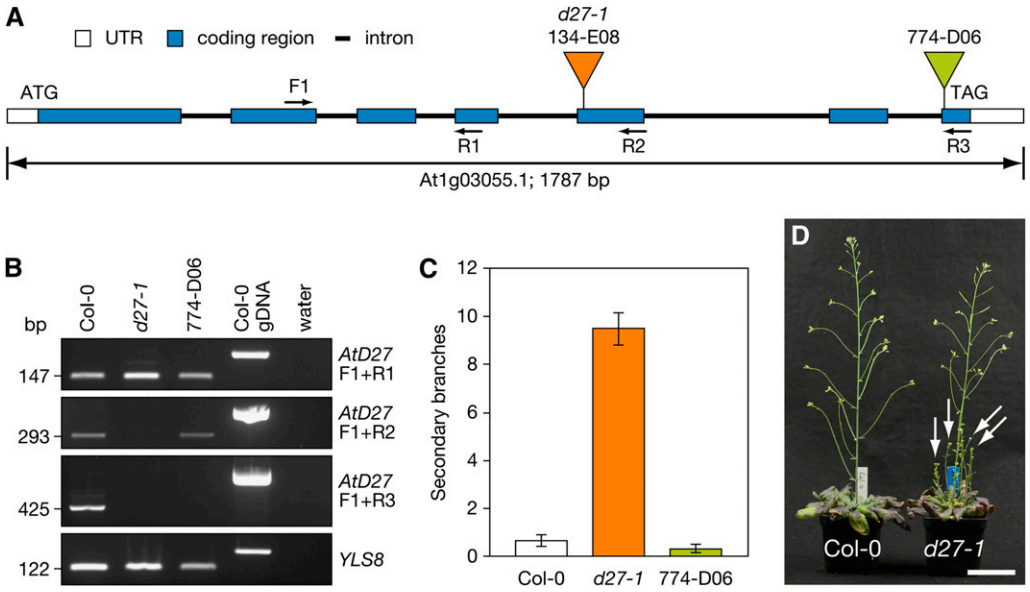

Figure 2. Arabidopsis *d27-1* mutants have increased axillary branching. A, Primary transcript structure of the Arabidopsis *D27* ortholog. Inverted triangles indicate the positions of T-DNA insertions in the two GABI-KAT lines, and arrows represent the approximate positions and orientations of PCR primers. UTR, Untranslated region. B, RT-PCR analysis of *D27* transcripts in seedlings homozygous for each T-DNA insertion allele. Primer pairs were selected to span each insertion point and an upstream region of the transcript. *YLS8* transcripts (*At5g08290*) serve as a control for RT. Amplification products from genomic DNA are larger due to intron sequences. C, Axillary rosette branches in Col-0 and individuals homozygous for each insertion allele. Data are means ± SE (n = 8–9 plants). D, Increased numbers of axillary branches (arrows) in *d27-1* mutants. Plants shown are 64 d old; they were grown under short days (8 h of light/16 h of dark) for 44 d and then transferred to continuous light for 20 d to induce flowering. Note the slightly dwarfed stature of *d27-1*. [See online article for color version of this figure.]

774D06 homozygotes had a normal branching pattern (Fig. 2, C and D). On the basis of its mutant phenotype, we named the GK-134E08 allele *d27-1* (hereafter referred to as *d27* for simplicity). The T-DNA insertion in *d27* disrupts the predicted protein at Leu-189, comparable to the nonfunctional protein produced in *Osd27*, which is disrupted after Gly-187 (Supplemental Fig. S1; Lin et al., 2009). These data suggest that *AtD27* is necessary for the regulation of axillary bud outgrowth and that the extreme 3′ end of the transcript is nonessential for the function of the resulting protein.

To confirm that the *d27* lesion was responsible for the increased branching phenotype, we complemented the mutant with a cDNA encoding the predicted D27 protein, expressed under the control of the cauliflower mosaic virus *35S* promoter. We isolated four independent transgenic lines, in which the transgene segregated in a ratio consistent with a single Mendelian locus and was expressed approximately 40-fold higher than in the wild type at the transcriptional level (Supplemental Fig. S2). In all four lines, the number of axillary branches and overall plant height were not significantly different from wild-type levels, fully complementing the *d27* phenotype (Fig. 3, A and B). We performed feeding experiments with GR24, a synthetic SL, to evaluate whether the increased branching phenotype of *d27* likely results from impaired SL biosynthesis, as is the case in rice (Lin et al., 2009). When grown in culture vessels on medium containing GR24, *d27* plants produced significantly fewer branches than those grown on control medium (Fig. 3C). The SL-deficient mutant *max3-11* exhibited a similar response, although its branching phenotype was more severe. In contrast, the SL-insensitive mutant *Atd14* showed no response at all to GR24, as demonstrated previously (Waters et al., 2012). A similar response to GR24 was seen with *d27* and *max3-9* plants grown hydroponically (Supplemental Fig. S3). Together, these data demonstrate that D27 is essential for the regulation of axillary branching and that branching inhibition in *d27* is limited by SL content rather than SL response.

D27 Acts Upstream of MAX1 in the SL Biosynthetic Pathway

Grafting wild-type rootstocks to *max1*, *max3*, or *max4* scions restores a wild-type branching pattern to the mutant shoots (Booker et al., 2005). This outcome results from the graft transmission of root-synthesized SL to the shoot presumably via the transpiration stream (Foo et al., 2001; Kohlen et al., 2011). Conversely, grafting with these lines shows that SL biosynthesis also occurs in the shoot, as wild-type shoots have wild-type branching phenotypes even where grafted with mutant rootstocks. To verify that *d27*

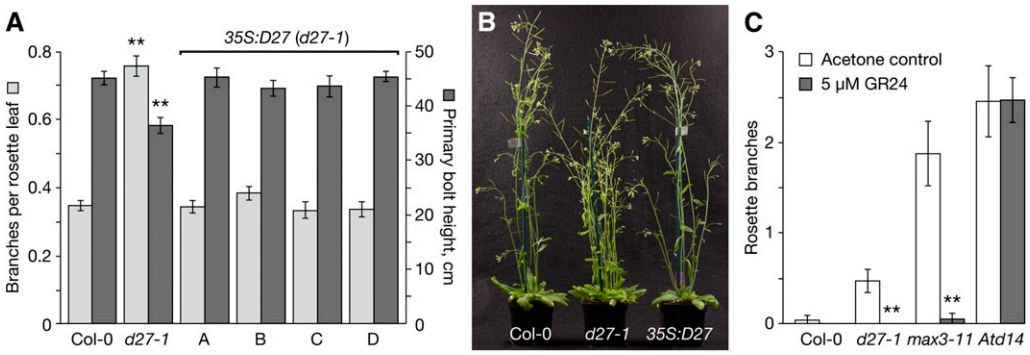

Figure 3. Arabidopsis D27 is involved in SL-mediated repression of shoot branching. A, Branch numbers (light gray bars) and plant height (dark gray bars) in 42-d-old Col-0, *d27-1*, and four complemented lines, A to D. Data are means ± SE (n = 7–9 plants). Asterisks denote significant differences from Col-0 ($P < 0.01$, one-way ANOVA). B, Axillary branching in the representative plants described in A. C, Effect of GR24 on branching in 32-d-old plants grown in Phytatrays. Data are means ± SE (n = 13–67 plants). Asterisks denote significant differences between treated and untreated samples within the same genotype (two-tailed Mann-Whitney U test, $P < 0.01$). [See online article for color version of this figure.]

shoots are similarly responsive to a graft-transmissible signal, we generated reciprocal grafts between wild-type ecotype Columbia (Col-0) and *d27* and found that wild-type rootstocks could suppress the increased branching phenotype of *d27* shoots (Fig. 4). A mutant rootstock had no effect on the phenotype of a wild-type shoot, showing that *D27* expression in the shoot is sufficient to inhibit branching (Fig. 4).

It has been shown previously that MAX1 operates downstream of MAX3 and MAX4 in SL biosynthesis, because a *max1* rootstock can restore a wild-type branching pattern to *max3* and *max4* shoots, but not vice versa (Booker et al., 2005). These findings have also demonstrated that a compound intermediate between MAX3/MAX4 and MAX1 is subject to long-distance transport from the root to the shoot. Likewise, the substrates of MAX3 and MAX4 are nonmobile (or are unable to access MAX3/MAX4 in the plastid of a remote cell), because a *max3* rootstock fails to complement a *max4* shoot, and vice versa (Booker et al., 2005). To investigate the relative position of D27 within the MAX pathway, we generated reciprocal grafts between *d27* and either *max1* or *max4*. A *max1* rootstock was able to fully restore the branching phenotype of a *d27* shoot, demonstrating that MAX1 operates downstream of D27 (Fig. 4). Interestingly, as for *max4* discussed below, the branching of *max1* scions grafted to *d27* rootstocks was reduced to that of *d27* self-grafts (Fig. 4). This suggests that *d27* may generate a small amount of SL, or a substance that can partly compensate for SL deficiency, and is consistent with the relatively mild branching phenotype of *d27* compared with *max1*, *max3*, and *max4* (Figs. 3C and 4; Supplemental Fig. S3).

In contrast to graft combinations involving *d27* with the wild type or *max1*, reciprocal grafts between *d27* and *max4* failed to restore branching to wild-type levels in either mutant shoot (Fig. 4; Sorefan et al., 2003; Hayward et al., 2009). This situation is similar to grafts between the carotenoid cleavage dioxygenase mutants of Arabidopsis (*max3* and *max4*) and pea (*Pisum sativum*; *rms1* and *rms5*), which, unlike grafts with wild-type partners, are unable to show branching inhibition (Morris et al., 2001; Booker et al., 2005). As discussed below, this is consistent with D27 acting in the plastid on a plastid-localized, nonmobile substrate. Unlike grafts between *max3* and *max4*, *max4* rootstocks caused a slight enhancement of branching in *d27* shoots and *d27* rootstocks caused a slight reduction of branching in *max4* shoots. As *d27* has an intermediate branching phenotype compared with *max4* (Fig. 4), *d27* presumably has elevated graft-transmissible hormone content compared with *max4*. In summary, these grafting

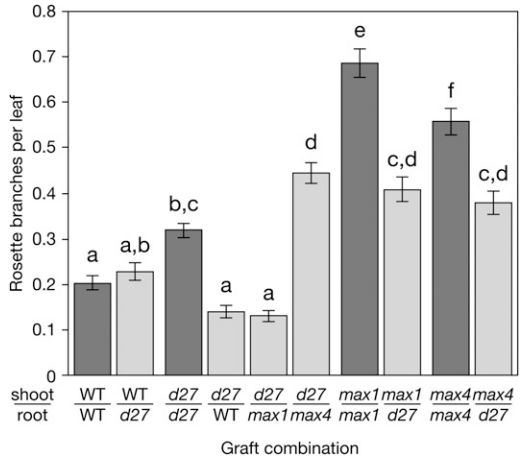

Figure 4. D27 acts upstream of MAX1 in the SL biosynthetic pathway. Values shown are numbers of rosette branches per leaf in grafted plants. Dark gray bars represent self-graft controls. Data are means ± SE (n = 22–34 plants). Values with the same lowercase letter are not significantly different from one another (one-way ANOVA, $P < 0.05$). WT, Wild type.

data are consistent with D27 functioning upstream of MAX1 in the biosynthesis of SL.

AtD27 Is Localized to the Plastid

Given the apparent nonmobility of the D27 precursor and the biochemical function of D27, it is likely that the Arabidopsis D27 protein is spatially restricted to the plastid. To determine the likely cellular location of D27, we generated a chimeric construct encoding the full-length D27 protein fused to the N terminus of GFP. Following transient expression in onion (*Allium cepa*) epidermis, the GFP fluorescence fully overlapped with the red fluorescence from the coexpressed plastid-specific marker (Fig. 5, A–D). No GFP fluorescence was detected beyond the plastid, suggesting that the full-length D27 protein was strictly localized to this organelle. This is in accord with plastid localization of OsD27 (Lin et al., 2009). The D27 protein encodes a predicted N-terminal plastid transit peptide of 47 amino acids (Supplemental Fig. S1). To test whether this presequence is sufficient to direct plastid localization, we generated a translational fusion between the first 50 amino acids of D27 and GFP and subjected onion epidermal cells to transient transformation as before. Again, the fluorescence signals from both the GFP and the plastid-specific marker fully overlapped (Fig. 5, E–H), indicating that D27 possesses a bona fide plastid transit peptide. Together, these data suggest that D27 functions in the plastid, consistent with the demonstrated cellular location of OsD27 in rice and its anticipated activity on a nonmobile precursor.

D27 Transcripts Are Subject to Auxin and Feedback Control

D27, *MAX3*, and *MAX4* transcript abundance from public microarray data revealed potential differential expression intensities throughout the plant, with a relative deficit of *D27* in root tissue (Supplemental Fig. S4). Quantitative RT-PCR analysis of Col-0 tissues confirmed that *D27* transcripts were more abundant in shoot tissue than in roots of 3-week-old wild-type plants, while *MAX3* and *MAX4* transcripts accumulated most strongly in the hypocotyl and roots (Fig. 6A). In contrast, *MAX1* transcript levels varied little over the tissues examined. Consistent with their role in SL response, we found that *MAX2* and *AtD14* transcripts were evenly expressed across the shoot, hypocotyl, and root (Fig. 6A). Differential spatial expression of *D27* compared with *MAX3* and *MAX4* then led us to investigate whether *D27* was under similar feedback control as *MAX3* and *MAX4*.

In all *max* mutants, levels of *MAX3* and *MAX4* transcripts in the hypocotyl are 6- to 10-fold higher than in the wild type, indicative of feedback up-regulation (Hayward et al., 2009). This feedback process is dependent on a combination of auxin and nonauxin

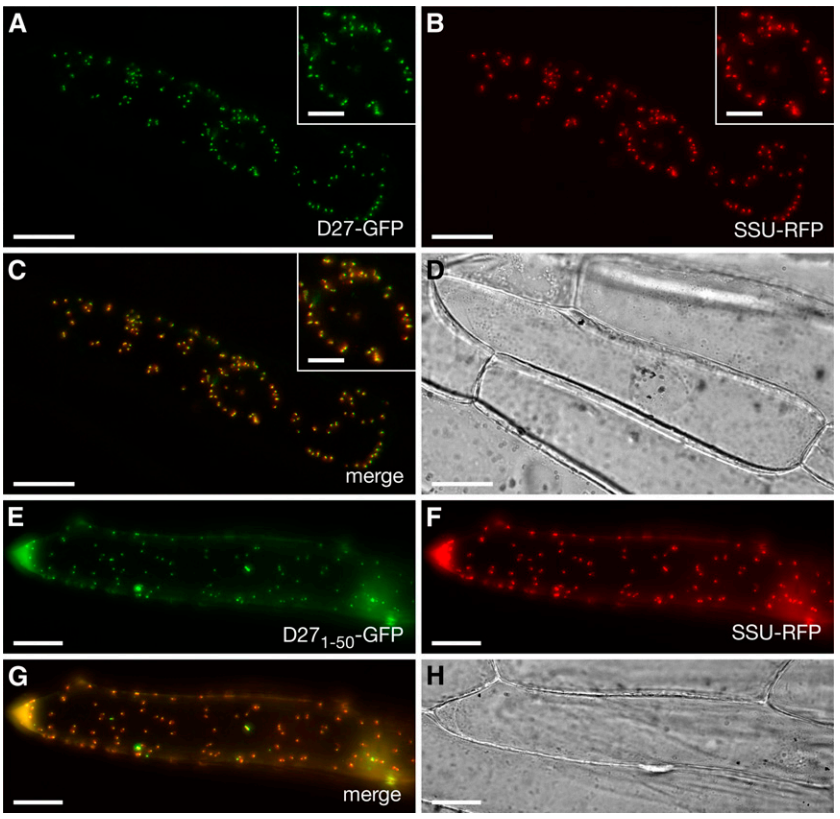

Figure 5. The N terminus of Arabidopsis D27 is sufficient for plastid targeting. A and E, Epifluorescence micrographs of onion epidermis transiently transformed with plasmids encoding a full-length D27-GFP protein fusion (A) or the first 50 amino acids of D27 fused to the N terminus of GFP (E). B and F, Plastids are positively identified by coexpression of a protein fusion between the full-length Rubisco small subunit from pea (SSU) and RFP. C and G, The merged images confirm colocalization of the two fluorescent signals. Insets in A to C provide magnification and show clustering of plastids around the cell nucleus. D and H, Bright-field micrographs of the same field of view to provide the cell outline. Bars = 50 μm (main images) and 20 μm (insets).

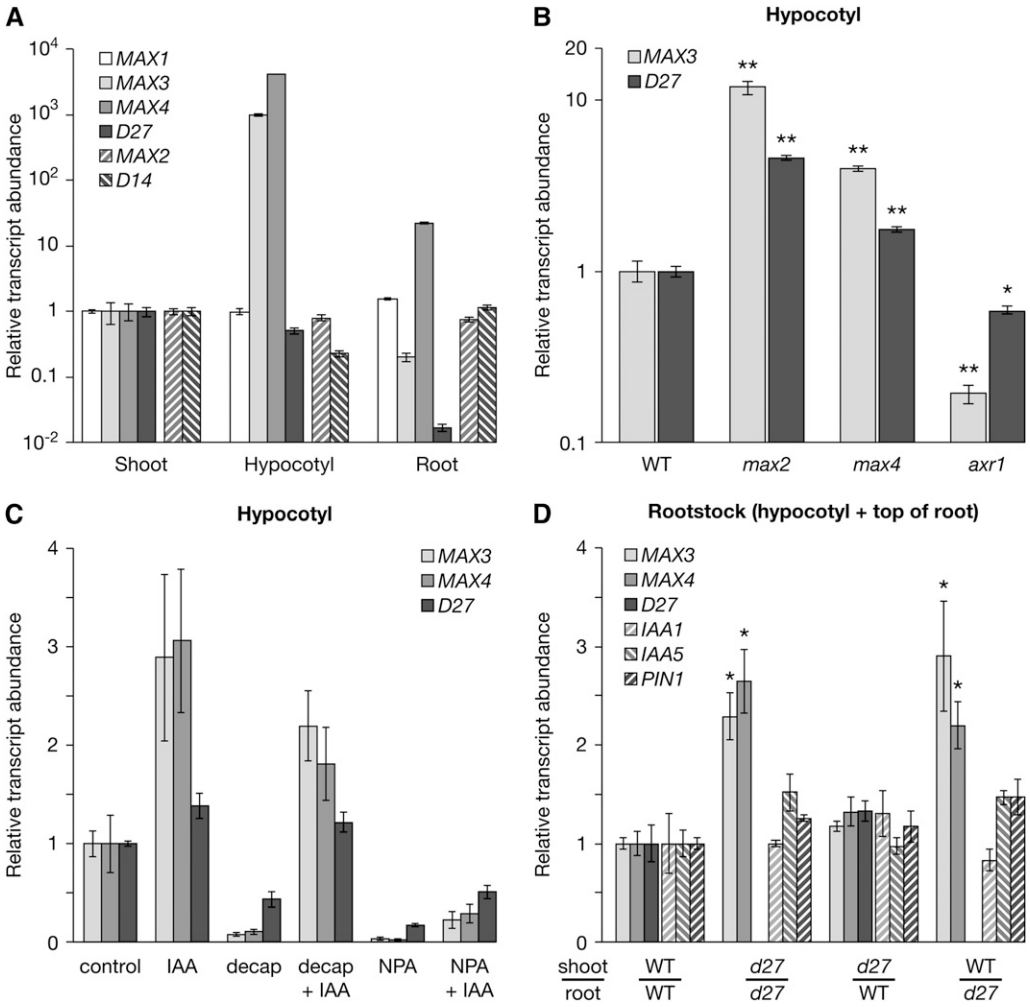

Figure 6. *D27* transcripts are sensitive to auxin and feedback regulation. A, Accumulation of SL- and auxin-related transcripts in shoots (leaves and stem above the cotyledons), hypocotyls, and roots of wild-type plants grown hydroponically for 3 weeks. Transcripts were normalized to *TIP41L* (*At4g34270*) and scaled to the value in the shoot sample. Data are means ± SE ($n = 3$ pools of 8–10 plants). B, *MAX3* and *D27* transcript accumulation in hypocotyls of soil-grown, prebolting plants of the indicated genotypes, as measured by quantitative RT-PCR. Transcripts were normalized to the combined expression of three *ACTIN* genes (*At3g18780*, *At5g09810*, and *At1g49240*) and scaled relative to the expression level in Col-0. Data are means ± SE ($n = 4$ pools of approximately 20 plants). C, Auxin-dependent regulation of *MAX3*, *MAX4*, and *D27* transcript levels in hypocotyls of 17-d old, soil-grown wild-type plants. Treatments are as follows: IAA addition (in a lanolin ring around the top of the hypocotyl); decapitation (decap); decapitation and IAA addition (in lanolin added to the stump); addition of the auxin transport inhibitor NPA (in a lanolin ring around the top of the hypocotyl); and combined addition of IAA and NPA (together in a lanolin ring around the top of the hypocotyl). Treatment time was 4 h. Data are means ± SE ($n = 3$ pools of approximately 20 plants per pool), normalized to *ACTIN* and scaled as above. D, SL- and auxin-related gene expression in rootstocks of reciprocal grafts between the Col-0 wild type (WT) and *d27-1*. For each shoot/rootstock combination, hypocotyl and upper root tissue was harvested below the graft union. Data are means ± SE ($n = 3$ pools of approximately 4 plants per pool), normalized to *ACTIN* and scaled as above. Values for *D27* transcripts in *d27-1* mutants were omitted. They were 13.8- ± 0.8-fold higher than in Col-0, but this difference is not biologically meaningful because the mutation may affect transcript processing and/or stability. The quantitative PCR primers for *D27* are located upstream of the T-DNA insertion site. Asterisks denote significant differences from Col-0 (* $P < 0.05$, ** $P < 0.01$, one-way ANOVA).

signals. SL-related auxin responses require the AUXIN RESISTANT1 (AXR1) protein, as *axr1* auxin response mutants have reduced *MAX3* and *MAX4* transcript levels, at least in cauline internodes and hypocotyls of 5-week-old plants (Hayward et al., 2009). In hypocotyls of 3-week-old prebolting *max2* and *max4* mutants, *D27* transcripts were significantly up-regulated relative to the wild type (Fig. 6B). However, these changes were typically half the increase observed for *MAX3* transcripts, which were over 10-fold and 5-fold up-regulated in a *max2* and *max4* background, respectively (Fig. 6B). Likewise, while *MAX3* transcripts

were 5-fold down-regulated in *axr1* mutants, *D27* transcripts were only moderately (albeit significantly) less abundant. Consequently, although the magnitude of expression changes for *D27* are less than for *MAX3*, the response is similar and therefore may involve common regulatory components.

Levels of *MAX3* and *MAX4* transcripts in the hypocotyl decrease in response to removal of the shoot tip (decapitation) by decreasing expression levels (Hayward et al., 2009). This presumably reduces SL levels in order to allow buds below the decapitation site to grow and compensate for the missing shoot tip. A proportion of the decrease in gene expression is due to auxin depletion in the hypocotyl after removal of the shoot tip (the shoot tip being the main source of auxin for the plant). We checked *D27* gene expression in hypocotyls after various treatments known to modulate auxin content: auxin (indole-3-acetic acid [IAA]) addition; decapitation; decapitation followed by IAA addition; addition of the auxin transport inhibitor *N*-1-naphthylphthalamic acid (NPA); and combined addition of IAA and NPA. *D27* expression showed similar trends to that of *MAX3* and *MAX4* across these treatments, although, as above, the magnitude of the response was less (Fig. 6C). Classical auxin-responsive genes, *IAA1*, *IAA5*, and *PIN1*, also responded in a similar manner in these samples, but with varied magnitudes (Supplemental Fig. S5). The only difference between trends among the treatments for the classical auxin response genes compared with the SL genes was that exogenous IAA added to NPA-treated plants fully restored and indeed overcompensated for the NPA, whereas the SL genes were not fully restored back to control levels in this IAA+NPA treatment. This raises the possibility of auxin and nonauxin effects of NPA regulation of *MAX3*, *MAX4*, and *D27* gene expression.

In pea, there is evidence that feedback regulation of *MAX3* and *MAX4* orthologs can occur over long distances in a graft-transmissible and localized manner (Foo et al., 2005; Johnson et al., 2006; Dun et al., 2009b). In Arabidopsis, a wild-type shoot can suppress the elevated *MAX3* and *MAX4* expression in a *max2* rootstock (Hayward et al., 2009), indicative of a downwardly mobile feedback signal. Nevertheless, in Arabidopsis, the local effect of *max2* in the rootstock is greater than that of the long-distance signaling from shoots. In similar experiments in pea, the effect of the scion appears greater than the local effect of the rootstock (Foo et al., 2005; Johnson et al., 2006). In contrast to SL response mutants, grafts between the wild type and SL-deficient mutants in pea show a minor effect of the scion on gene expression in the rootstock, possibly due to the restoration of SL content by the wild-type graft partner. To investigate the scenario for *d27*, we analyzed gene expression in the hypocotyl and rootstock of plants reciprocally grafted with the wild type (Fig. 6D). In *d27* self-grafts, *MAX3* and *MAX4* transcripts were up-regulated, consistent with feedback. (*D27* transcripts were also highly overexpressed, but this may be primarily a result of misregulation of a nonfunctional transcript.) As with wild-type rootstocks of pea grafted to mutants in SL biosynthesis (Dun et al., 2009b), expression in the root was not significantly affected by the genotype of the shoot in either reciprocal graft in Arabidopsis. As in pea, this may be because wild-type rootstocks can restore branching, and presumably the long-distance feedback signal, to normal levels in *d27* shoots. Notably, in grafts involving *d27*, the three auxin-responsive transcripts did not exhibit a statistically significant difference from wild-type self-grafts, suggesting that auxin transport and/or signaling is not substantially affected in *d27* mutants. This outcome may be due to the relatively moderate phenotype of *d27*.

DISCUSSION

The identification of AtD27 as the ortholog of OsD27 is supported by phenotypic, physiological, and genetic data. From a genetic point of view, we identified the sequence with greatest similarity to OsD27 (Fig. 1; Supplemental Fig. S1), obtained homozygous T-DNA insertion *Atd27* mutant lines (Fig. 2), and complemented this mutant phenotype to the wild type with overexpression of *AtD27* (Fig. 3; Supplemental Fig. S2). Like the *d27* mutant in rice, *Atd27* affects the number of axillary shoots and plant height (Fig. 3). Interestingly, the *Atd27* mutant is also similar to *Osd27* in the sense that both mutants are intermediate in phenotype compared with their respective wild types and other characterized SL mutants (Fig. 3). As expected, *Atd27* responds to GR24 supplied through the roots (Fig. 3; Supplemental Fig. S3).

Our phylogenetic analysis demonstrates that AtD27 belongs to a wider family of proteins that originated early in the evolution of photosynthetic eukaryotes. Although D27-like proteins are found throughout cyanobacteria and green algae, two clades are strictly specific to land plants. Notably, CCD7 (MAX3) and CCD8 (MAX4) form monophyletic clades in land plants, and putative orthologs of both CCD7 and CCD8 are present in *Chlamydomonas reinhardtii* and other photosynthetic eukaryotes (Ledger et al., 2010; Vallabhaneni et al., 2010; Proust et al., 2011). Thus, the enzymatic machinery necessary for the early steps of SL biosynthesis may have been present in the ancestors of the land plants. Interestingly, all land plants so far examined possess homologs of the proteins required for SL response (i.e. MAX2 and D14), but so far, no homologs have been found in other photosynthetic eukaryotes, including the streptophyte algae, the closest living relatives of the land plants (Waters et al., 2011, 2012). Although this finding could reflect incomplete genome sequence data for the streptophyte algae, it is possible that SL signaling coincided with the evolution of the land plants and the concurrent development of complex body plans. As carotenoids are essential pigments associated with light harvesting and photoprotection in oxygenic

photosynthetic organisms, carotenoid metabolism is a fundamental requirement for photosynthesis and likely the original function of CCD7-, CCD8-, and D27-like proteins. As multicellularity evolved, we propose that gene duplications permitted the acquisition of novel gene function, and a separate pathway for carotenoid breakdown was co-opted for signaling purposes. Recently, SLs were shown to have a dramatic role in gametophytic development of the moss *P. patens*. Loss of PpCCD8 activity leads to severely compromised SL profiles and impaired control of protonemal branching, which in turn limits the ability to sense neighboring colonies (Proust et al., 2011). As the *P. patens* genome also encodes a D27 ortholog, multiple D14 homologs, and a single MAX2 ortholog, it appears that the SL biosynthesis and signaling system is conserved among land plants. The availability of complete genome sequences for the streptophyte algae, combined with an assessment of their ability to produce SLs, will help in determining the origin of SL signaling.

We have contributed further to the understanding of the D27 protein by demonstrating that the Arabidopsis version of D27 functions upstream of MAX1 in the production of SL-related signal(s) and displays similar feedback control compared with other genes encoding plastid-localized SL biosynthesis proteins. *AtD27* controls a graft-transmissible signal because branching can be inhibited in *Atd27* mutant shoots by grafting to wild-type rootstocks (Fig. 4). Whereas *max1* mutant rootstocks retain this inhibitory function, *max4* rootstocks do not. This is clear evidence in support of D27 acting upstream of MAX1. On the other hand, the grafting data do not permit the ordering of D27 with respect to MAX4, presumably because the carotenoid-derived substrates of D27 and MAX4 are unable to leave the plastid (Alder et al., 2012). Similarly, the relationship between MAX3 and MAX4 could not be determined via grafting (Booker et al., 2005). Instead, biochemical studies have shown that MAX3/CCD7 and MAX4/CCD8 likely act sequentially in carotenoid cleavage (Schwartz et al., 2004). The precise functions of MAX3 and MAX4 were only recently elucidated following the identification of D27 as a β-carotene isomerase (Alder et al., 2012). In vitro, the combination of purified D27, CCD7, and CCD8 is sufficient to convert β-carotene into carlactone, while exogenous carlactone is sufficient to rescue the high-tillering phenotype of rice *d27*, *ccd7*, and *ccd8* mutants (Alder et al., 2012). Thus, there are at least three enzymatic steps in the plastid before the generation of a mobile SL precursor (Fig. 7). These findings are consistent with our grafting studies. At present, it is unclear whether carlactone itself can exit the plastid and mobilize and whether further modifications by subsequent enzymes are required for the transport of the branching signal from root to shoot.

Like the *d27* mutant in rice, which is substantially SL deficient, the Arabidopsis *d27-1* shows a weaker

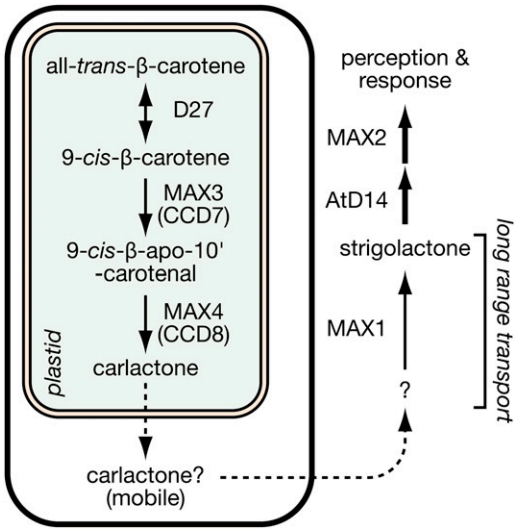

Figure 7. Position of D27 within the SL biosynthesis and signaling pathway. Enzymatic steps are denoted with solid arrows, transport steps with dashed arrows, and signaling steps with thick arrows. AtD14 may be a SL receptor, a hydrolytic enzyme that processes SL into a further active compound, or a combination of both; for a discussion, see Scaffidi et al. (2012). [See online article for color version of this figure.]

phenotype than other branching mutants in the MAX/D/RMS pathway. Our grafting studies support the notion of residual bioactive branching inhibition capacity in *d27*, because *d27* rootstocks can partly inhibit branching in *max1* and *max4* scions down to the level of *d27* control plants (Fig. 4). Based on our phylogenetic analysis, it is possible that another D27-like protein can perform the isomerization of all-trans-β-carotene in the absence of functional D27. Although the function of *At1g64680* is unknown, the predicted protein has been localized to the chloroplast envelope and/or thylakoids by liquid chromatography-tandem mass spectrometry analysis (Ferro et al., 2010), while its closest homolog in rice, encoded by *Os08g0114100*, is weakly predicted to be plastidic by TargetP software (Emanuelsson et al., 2007). Alternatively, nonenzymic isomerization may provide a small amount of 9-cis-β-carotene substrate for MAX3/CCD7, allowing only limited levels of SL to be synthesized in the *d27* mutant (despite enhanced *MAX3* and *MAX4* expression). However, the rice *d27* mutant does not contain any detectable SL, either by liquid chromatography-mass spectrometry or a bioassay based on *Orobanche* seed germination (Lin et al., 2009), which may suggest that any residual SLs are below the limit of detection in *d27*. On the other hand, *max1* and *max4* mutants, which exhibit a strong branching phenotype, still contain detectable levels of orobanchol (Kohlen et al., 2011). This contradiction means that the basis for the relatively mild branching phenotype of *d27* in both rice and Arabidopsis is currently unclear. Therefore, detailed biochemical analyses of the *d27*

mutant, intact or grafted, compared with other mutant and wild-type lines may be useful in evaluation of the levels and profiles of endogenous SLs and their potential correlations with phenotypic responses.

Interestingly, despite the complete rescue of *d27* shoots by grafting to wild-type rootstocks, the expression of D27 is not greatest in the rootstock. Indeed, its expression in roots and hypocotyls of 3-week-old plants is greatly and slightly reduced, respectively, compared with shoots (Fig. 6A). This regulation is a point of difference with *MAX3* and *MAX4*, which are both highly expressed in the hypocotyl. In a further contrast, *MAX3* is relatively weakly expressed in roots compared with shoots, while *MAX4* is again highly expressed. The expression patterns that we observed are fully consistent with meta-profiles derived from multiple microarray experiments (Supplemental Fig. S4). Recently, it was found that two GRAS-type transcription factors, NSP1 and NSP2, regulate *D27* expression and SL levels in *Medicago* and rice (Liu et al., 2011). In *Medicago*, the *nsp1* mutant does not produce any detectable SL while the *nsp2* mutant exhibits a specific deficiency in didehydro-orobanchol, and these deficiencies correlate with a decrease in *MtD27* transcripts in both mutants. Interestingly, *MtCCD7* and *MtCCD8* expression was unaffected in *nsp1* and *nsp2* mutants (Liu et al., 2011), suggesting that the carotenoid cleavage steps in SL biosynthesis are under distinct transcriptional control from the initial isomerization step involving D27. This finding is consistent with our data from Arabidopsis. Although it is unclear whether *MtD27* transcription is directly regulated by NSP1 and NSP2, the conservation between rice and *Medicago* of this regulatory system implies that a similar mechanism might operate in Arabidopsis and beyond. The identification of putative NSP1 and NSP2 orthologs in Arabidopsis (Zhu et al., 2006) opens the door for reverse genetics to address this question.

In contrast to the differences in relative expression among different tissues, the SL biosynthesis genes *D27*, *MAX3*, and *MAX4* show similar trends in response to auxin-related treatments and in different mutant backgrounds. Although *D27* transcripts show lower magnitudes of response across all experiments, they show similar trends to other SL biosynthesis transcripts. *D27* expression is enhanced in the hypocotyl in SL-deficient or SL response mutant backgrounds, and it appears to be up-regulated by auxin. The auxin response is indicated by reduced expression in *axr1* mutants and in response to auxin addition or depletion via decapitation and NPA treatment. As shown from grafted plants, *d27* mutants also show enhanced expression of *MAX3* and *MAX4*, which is again consistent with SL deficiency causing the up-regulation of these genes. Restoration of SL content in the mutant shoots by wild-type rootstocks means we cannot easily test whether a component of this feedback is graft transmissible (Hayward et al., 2009). However, the majority of the feedback induced by *d27* is likely to be local, since *d27* rootstocks cause high expression of *MAX3* and *MAX4* similar to mutant self-grafts even where the scion is the wild type.

The regulation by auxin of a third protein in the SL pathway further supports the hypothesis that SLs act downstream of auxin in the control of shoot branching (Brewer et al., 2009). However, again, very small increases in the expression of *PIN1* and *IAA5* in *d27* mutants (Fig. 6D) indicate enhanced auxin signaling or content, which could be indicative of enhanced auxin transport as observed in *Osd27* and several other branching mutants (Lin et al., 2009; Crawford et al., 2010; Domagalska and Leyser, 2011). We have recently modeled long-distance auxin transport in the stem, and these data, in addition to data on auxin transport under high auxin content, demonstrate that wild-type plants do not have reduced auxin transport capacity relative to SL mutants (Brewer et al., 2009; Renton et al., 2012). Rather, in those experiments, the enhanced auxin transport seen in *max3* and *max4* mutants was more likely to be due to enhanced uptake of the exogenously supplied radiolabeled auxin to the top of the long-distance polar auxin transport stream (Renton et al., 2012).

In summary, *d27* represents a new genetic tool for the elucidation of shoot branching mechanisms and their regulation in Arabidopsis. Together with MAX3 and MAX4, D27 acts in the plastid on the production of carlactone, an intermediate in the SL pathway, prior to MAX1. These genes encoding plastid-localized proteins, although expressed somewhat differently at the level of different plant parts, appear to carry conserved properties in terms of the regulation of their expression, particularly by the plant hormone auxin.

MATERIALS AND METHODS

Plant Material and Growth Conditions

The *Atd27-1* mutant was isolated from the GABI-Kat collection (GK-134E08.01) and obtained from the European Arabidopsis Stock Centre (NASC; identifier N761233). The second T-DNA insertion allele located at the 3′ end of *AtD27* was isolated from GK-774D06.06 (NASC identifier N762010). A third GABI-Kat line, GK-114A05, is annotated as carrying an insertion in the fifth intron of *At1g03055*, but we could not identify any individuals carrying a T-DNA at the expected location. T-DNA homozygotes were identified by PCR with the genomic primers MW277 (5′-TGGTCCCACCTTTGATCATT-3′) and MW278 (5′-TCTAATGCTTCACACCGTAGC-3′) and a T-DNA-specific primer, o8409 (5′-ATATTGACCATCATACTCATTGC-3′). Col-0, *max1-1*, *max2-1*, *max3-11*, *max4-1*, and *axr1-3* were from our laboratory stocks; Wassilewskija-4 (Ws-4; used for the results shown in Fig. 6C) and *max3-9* (N9567) were obtained from NASC (N5390). The *Atd14-1* mutant was described previously (Waters et al., 2012).

Unless otherwise stated, Arabidopsis (*Arabidopsis thaliana*) plants were grown under fluorescent lamps emitting 100 to 120 μmol photons s^{-1} m^{-2} (intensity at the rosette level) in a 6:1:1 mixture of peat, vermiculite, and perlite or in University of California mix with added 60% vermiculite. Plants from the Col-0 background were grown in a 16-h-light/8-h-dark photoperiod and a 22°C light/16°C dark temperature cycle, or in constant 22°C. Ws-4 was initially grown for 2 weeks in 14 h of light/10 h of dark and constant 18°C, in

order to compensate for the extreme early flowering in Ws-4 and to match their flowering time with Col-0.

Grafting and Branching Assays

Grafting of Arabidopsis seedlings was performed as described in Brosnan et al. (2007) and as described in Brewer et al. (2009). Treatment of plants with GR24 in Phytatrays was performed as described (Brewer et al., 2009). Treatment of plants grown in hydroponic medium has been described previously (Waters et al., 2012).

IAA Treatments

Prebolting Ws-4 plants were treated with a lanolin ring around the top of the hypocotyl containing 2.5% dimethyl sulfoxide and 2.5% ethanol (control) with 10 mM IAA and/or 10 mM NPA (an auxin transport inhibitor). Decapitation involved removing the apical meristem and some small leaves/flowers from the shoot apex of each plant. Hypocotyl tissue was harvested 4 h post treatment. Three replicates were used for each genotype, with approximately 20 plants used per replicate.

Generation of *35S:AtD27* Plants

RNA was isolated from 7-d-old whole seedlings using the Qiagen RNeasy procedure. cDNA was generated from 1 μg of total RNA using Invitrogen SuperScript III. The *At1g03055.1* coding sequence was first amplified using primers MW350 5′-AAAAAAGCAGGCT**ATG**AACACTAAGCTATCAC-3′ and MW351 5′-CAAGAAAGCTGGGT**CTA**ATGCTTCACACCGTAGC-3′ (translation initiation codon and stop codon, respectively, in boldface) using a proofreading DNA polymerase (Phusion; New England Biolabs). Approximately 250 pg of the PCR product was then reamplified using Gateway *attB* adapter primers 5′-GGGGACAAGTTTGTACAAAAAAGCAGGCT-3′ and 5′-GGGGACCACTTTGTACAAGAAAGCTGGGT-3′ (overlapping regions with MW350 and MW351, respectively, are underlined). The resulting PCR product was cloned into pDONR207 via Gateway-based recombination, and positive clones were confirmed by sequencing. The full-length coding sequence was then transferred to pMDC32 (Curtis and Grossniklaus, 2003) via recombination, generating the final *35S:D27* binary vector. The *d27-1* mutant was then transformed by the floral dip method. Transgenic seedlings were selected by growth in continuous light for 7 d on one-half-strength Murashige and Skoog medium containing 25 μg mL^{-1} hygromycin B.

Transient Transformation and Localization Studies

The full-length *D27* coding sequence was reamplified from pDONR207-D27 using primers MW350 and MW353 (5′-CAAGAAAGCTGGGTTATGCTTCACACCGTAGC-3′), in which the native stop codon was deleted. The region of *D27* encoding the plastid transit peptide was amplified using primers MW350 and MW352 (5′-CAAGAAAGCTGGGTTCTCTTTTGCAGCCTTGAG-3′). Both PCR products were then reamplified with the universal Gateway *attB* primers described above and cloned into pDONR207. Positive clones of each were then recombined with pMDC83 (Curtis and Grossniklaus, 2003) to generate clones expressing N-D27-mGFP6-C protein fusions. For colocalization, the full-length cDNA of the small subunit of Rubisco from pea (*Pisum sativum*) was fused to the N terminus of red fluorescent protein (RFP; Carrie et al., 2009).

Plasmids (5 μg) were precipitated onto 1-μm gold particles and biolistically transformed into onion (*Allium cepa*) epidermis as described previously (Thirkettle-Watts et al., 2003). Images were obtained with an Olympus BX61 epifluorescence microscope equipped with GFP (U-MGFPHQ) and RFP (U-MRFPHQ) filters and manipulated with Olympus cell^R software.

RT-PCR and Quantitative RT-PCR Analysis

Total RNA was extracted using the RNeasy (Qiagen) or NucleoSpin RNA Plant (Macherey-Nagel) procedure. For small tissue samples (Fig. 6D), a modified TRIzol (Invitrogen) procedure was used with subsequent RNeasy cleanup. Contaminating DNA was removed with Turbo DNA-*free* (Ambion) or DNase (Macherey-Nagel or Qiagen), and RNA was quantified with a NanoDrop 1000 spectrophotometer.

In the case of Figure 2B, Figure 6A, and Supplemental Figure S2C, cDNA was generated from 0.5 μg of total RNA in a 10-μL reaction using the iScript cDNA Synthesis kit (Bio-Rad). Quantitative RT-PCR was performed on a Roche LC480 using LightCycler 480 SYBR Green Master Mix (Roche) in 5-μL reactions. Cycle conditions were as follows: 95°C for 10 min; then 45 cycles of 95°C for 20 s, 60°C for 20 s, and 72°C for 20 s; followed by melt-curve analysis. Crossing point values were calculated under high confidence. For each biological replicate, two technical replicates of each real-time PCR were examined, and the mean crossing point value was used to calculate expression relative to an internal reference gene using the formula $(E_{gene})^{-Cp\_gene}/(E_{ref})^{-Cp\_ref}$, where E is the primer efficiency and Cp represents the crossing point. Primer efficiencies were determined in separate runs using serial dilutions of pooled cDNA. Reference genes were selected from those identified by Czechowski et al. (2005); for comparing several tissue types, we selected *TIP41-LIKE* (*At4g34270*), and for seedlings, we chose a clathrin adapter complex subunit, *CACS* (*At5g46630*).

For all other figures, cDNA was produced using SuperScript III (Invitrogen) with 1,700 ng (Fig. 6B), 170 ng (Fig. 6C; Supplemental Fig. S4), and 60 ng (Fig. 6D) of total RNA (20-μL reaction). Quantitative RT-PCR was performed on the 7900 Real-Time PCR System (Applied Biosystems) using SensiMix SYBR (Bioline) in 10-μL reactions. Cycle conditions were as follows: 95°C for 10 min; then 45 cycles of 95°C for 15 s and 60°C for 1 min; followed by melt-curve analysis. Cycle threshold values were calculated at 0.2 normalized reporter fluorescence using SDS 2.3 (Applied Biosystems), and correlation coefficients and PCR efficiencies were calculated with LinRegPCR (Ramakers et al., 2003). Average PCR efficiencies (E) excluded poorly correlated reactions. Expression was relative to *ACTIN* genes using the formula $(E_{gene})^{-CT\_gene}/(E_{ref})^{-CT\_ref}$, where CT represents the cycle threshold.

Primers for the RT-PCR analysis of *d27-1* mutant transcripts (Fig. 2B) are F1 (5′-TGGACAGAGCATTACCGACA-3′), R1 (5′-CTCTGTAACCTCAGTCTCCCTCAC-3′), R2 (5′-CTCCATGTAGATAGGCATTC-3′), R3 (5′-TCTAATGCTTCACACCGTAGC-3′), *YLS8*-F (5′-GGGATGAGACCTGTATGCAGATGGA-3′), and *YLS8*-R (5′-GCTCGTACATGGTGTTGAAGTCTGG-3′). Primer pairs for quantitative RT-PCR were designed using QuantPrime (http://quantprime.mpimp-golm.mpg.de/) or manually by eye, except for *MAX4*, *IAA1* (Hayward et al., 2009), and *ACTIN* (Brown et al., 2003). All quantitative RT-PCR primers are listed in Supplemental Table S1.

Phylogenetic Analysis

Protein sequences with significant homology to D27 were identified with BLASTP searches of GenBank protein databases using the rice (*Oryza sativa* ssp. *japonica*) D27 amino acid sequence as a query (http://www.ncbi.nlm.nih.gov). Over 90 sequences were identified with a highly significant E-value score (E^{-10} or smaller). To reduce the complexity of the analysis, 62 sequences were selected on the basis of wide taxonomic coverage while also providing sufficient support for each clade. Sequences were further screened for duplication and truncation. Full-length sequences were then aligned using MAFFT (http://mafft.cbrc.jp/alignment/software) using the default settings. The alignment was conservatively trimmed using PFAAT (http://pfaat.sourceforge.net) to remove regions of poor homology, including putative N-terminal plastid transit peptides that show poor conservation. MrBayes version 3.1.2 (Ronquist and Huelsenbeck, 2003) was used to infer Bayesian trees (random start tree, four chains of temperature 0.2 in each of four independent runs, WAG substitution matrices (Whelan and Goldman, 2001), and four discrete categories of γ-distribution substitution rate). Computational analysis was performed using CIPRES Science Gateway version 3.1 (http://www.phylo.org/), and phylograms were generated using Dendroscope version 2.7.4 (http://www-ab.informatik.uni-tuebingen.de/software/dendroscope).

Statistical Analysis

For comparisons between multiple treatments and a control, one-way two-sided ANOVAs (Dunnett's t test) were performed as described in the figure legends. The overdispersed data shown in Figure 3C were analyzed using the more appropriate nonparametric Mann-Whitney U tests. When transcript expression data spanned several orders of magnitude (Fig. 6A), data were log transformed prior to analysis to control for large differences in variance between groups. Statistical analysis was performed with SAS Enterprise Guide 4.3.

Sequence data from this article can be found in the GenBank/EMBL data libraries under accession number NM_202019.1 (AtD27). Protein accession numbers are listed in Supplemental Table S2.

Supplemental Data

The following materials are available in the online version of this article.

Supplemental Figure S1. Alignment of selected D27 orthologs from angiosperms.

Supplemental Figure S2. Characterization of *35S:D27* transgenic lines.

Supplemental Figure S3. Axillary branching in *d27-1* mutants is suppressed by GR24.

Supplemental Figure S4. Meta-analysis of *D27*, *MAX3*, and *MAX4* transcript abundance in Arabidopsis tissues.

Supplemental Figure S5. Response of auxin-related transcripts to IAA, decapitation, and NPA treatments.

Supplemental Table S1. Primers used for quantitative RT-PCR.

Supplemental Table S2. List of protein sequences used in phylogeny reconstruction.

ACKNOWLEDGMENTS

We thank Adrian Scaffidi (University of Western Australia) for the synthesis of GR24 and for insightful discussion. We thank Kerry Condon Stephanie Kerr, and Sathyapriya Gunaseelan (University of Queensland) for assistance with plant growth, David Nelson (University of Georgia) for assistance with grafting, and Elizabeth Dun (University of Queensland) for valuable discussion.

Received February 23, 2012; accepted May 17, 2012; published May 22, 2012.

LITERATURE CITED

Agusti J, Herold S, Schwarz M, Sanchez P, Ljung K, Dun EA, Brewer PB, Beveridge CA, Sieberer T, Sehr EM, et al (2011) Strigolactone signaling is required for auxin-dependent stimulation of secondary growth in plants. Proc Natl Acad Sci USA **108:** 20242–20247

Akiyama K, Matsuzaki K-i, Hayashi H (2005) Plant sesquiterpenes induce hyphal branching in arbuscular mycorrhizal fungi. Nature **435:** 824–827

Alder A, Jamil M, Marzorati M, Bruno M, Vermathen M, Bigler P, Ghisla S, Bouwmeester H, Beyer P, Al-Babili S (2012) The path from β-carotene to carlactone, a strigolactone-like plant hormone. Science **335:** 1348–1351

Arite T, Iwata H, Ohshima K, Maekawa M, Nakajima M, Kojima M, Sakakibara H, Kyozuka J (2007) DWARF10, an RMS1/MAX4/DAD1 ortholog, controls lateral bud outgrowth in rice. Plant J **51:** 1019–1029

Arite T, Umehara M, Ishikawa S, Hanada A, Maekawa M, Yamaguchi S, Kyozuka J (2009) d14, a strigolactone-insensitive mutant of rice, shows an accelerated outgrowth of tillers. Plant Cell Physiol **50:** 1416–1424

Bennett T, Sieberer T, Willett B, Booker J, Luschnig C, Leyser O (2006) The Arabidopsis MAX pathway controls shoot branching by regulating auxin transport. Curr Biol **16:** 553–563

Booker J, Sieberer T, Wright W, Williamson L, Willett B, Stirnberg P, Turnbull C, Srinivasan M, Goddard P, Leyser O (2005) MAX1 encodes a cytochrome P450 family member that acts downstream of MAX3/4 to produce a carotenoid-derived branch-inhibiting hormone. Dev Cell **8:** 443–449

Brewer PB, Dun EA, Ferguson BJ, Rameau C, Beveridge CA (2009) Strigolactone acts downstream of auxin to regulate bud outgrowth in pea and Arabidopsis. Plant Physiol **150:** 482–493

Brosnan CA, Mitter N, Christie M, Smith NA, Waterhouse PM, Carroll BJ (2007) Nuclear gene silencing directs reception of long-distance mRNA silencing in Arabidopsis. Proc Natl Acad Sci USA **104:** 14741–14746

Brown RL, Kazan K, McGrath KC, Maclean DJ, Manners JM (2003) A role for the GCC-box in jasmonate-mediated activation of the PDF1.2 gene of Arabidopsis. Plant Physiol **132:** 1020–1032

Carrie C, Kühn K, Murcha MW, Duncan O, Small ID, O'Toole N, Whelan J (2009) Approaches to defining dual-targeted proteins in Arabidopsis. Plant J **57:** 1128–1139

Cook CE, Whichard LP, Turner B, Wall ME, Egley GH (1966) Germination of witchweed (Striga lutea Lour.): isolation and properties of a potent stimulant. Science **154:** 1189–1190

Crawford S, Shinohara N, Sieberer T, Williamson L, George G, Hepworth J, Müller D, Domagalska MA, Leyser O (2010) Strigolactones enhance competition between shoot branches by dampening auxin transport. Development **137:** 2905–2913

Curtis MD, Grossniklaus U (2003) A Gateway cloning vector set for high-throughput functional analysis of genes in planta. Plant Physiol **133:** 462–469

Czechowski T, Stitt M, Altmann T, Udvardi MK, Scheible W-R (2005) Genome-wide identification and testing of superior reference genes for transcript normalization in Arabidopsis. Plant Physiol **139:** 5–17

Domagalska MA, Leyser O (2011) Signal integration in the control of shoot branching. Nat Rev Mol Cell Biol **12:** 211–221

Dor E, Joel DM, Kapulnik Y, Koltai H, Hershenhorn J (2011) The synthetic strigolactone GR24 influences the growth pattern of phytopathogenic fungi. Planta **234:** 419–427

Dun EA, Brewer PB, Beveridge CA (2009a) Strigolactones: discovery of the elusive shoot branching hormone. Trends Plant Sci **14:** 364–372

Dun EA, Hanan J, Beveridge CA (2009b) Computational modeling and molecular physiology experiments reveal new insights into shoot branching in pea. Plant Cell **21:** 3459–3472

Emanuelsson O, Brunak S, von Heijne G, Nielsen H (2007) Locating proteins in the cell using TargetP, SignalP and related tools. Nat Protoc **2:** 953–971

Ferro M, Brugière S, Salvi D, Seigneurin-Berny D, Court M, Moyet L, Ramus C, Miras S, Mellal M, Le Gall S, et al (2010) AT_CHLORO, a comprehensive chloroplast proteome database with subplastidial localization and curated information on envelope proteins. Mol Cell Proteomics **9:** 1063–1084

Foo E, Bullier E, Goussot M, Foucher F, Rameau C, Beveridge CA (2005) The branching gene RAMOSUS1 mediates interactions among two novel signals and auxin in pea. Plant Cell **17:** 464–474

Foo E, Turnbull CG, Beveridge CA (2001) Long-distance signaling and the control of branching in the rms1 mutant of pea. Plant Physiol **126:** 203–209

Gomez-Roldan V, Fermas S, Brewer PB, Puech-Pagès V, Dun EA, Pillot J-P, Letisse F, Matusova R, Danoun S, Portais J-C, et al (2008) Strigolactone inhibition of shoot branching. Nature **455:** 189–194

Hayward A, Stirnberg P, Beveridge C, Leyser O (2009) Interactions between auxin and strigolactone in shoot branching control. Plant Physiol **151:** 400–412

Johnson X, Brcich T, Dun EA, Goussot M, Haurogné K, Beveridge CA, Rameau C (2006) Branching genes are conserved across species: genes controlling a novel signal in pea are coregulated by other long-distance signals. Plant Physiol **142:** 1014–1026

Kapulnik Y, Delaux P-M, Resnick N, Mayzlish-Gati E, Wininger S, Bhattacharya C, Séjalon-Delmas N, Combier J-P, Bécard G, Belausov E, et al (2011) Strigolactones affect lateral root formation and root-hair elongation in Arabidopsis. Planta **233:** 209–216

Kleinboelting N, Huep G, Kloetgen A, Viehoever P, Weisshaar B (2012) GABI-Kat SimpleSearch: new features of the Arabidopsis thaliana T-DNA mutant database. Nucleic Acids Res **40:** D1211–D1215

Kohlen W, Charnikhova T, Liu Q, Bours R, Domagalska MA, Beguerie S, Verstappen F, Leyser O, Bouwmeester H, Ruyter-Spira C (2011) Strigolactones are transported through the xylem and play a key role in shoot architectural response to phosphate deficiency in nonarbuscular mycorrhizal host Arabidopsis. Plant Physiol **155:** 974–987

Ledger SE, Janssen BJ, Karunairetnam S, Wang T, Snowden KC (2010) Modified CAROTENOID CLEAVAGE DIOXYGENASE8 expression correlates with altered branching in kiwifruit (Actinidia chinensis). New Phytol **188:** 803–813

Lin H, Wang R, Qian Q, Yan M, Meng X, Fu Z, Yan C, Jiang B, Su Z, Li J, et al (2009) DWARF27, an iron-containing protein required for the biosynthesis of strigolactones, regulates rice tiller bud outgrowth. Plant Cell **21:** 1512–1525

Liu W, Kohlen W, Lillo A, Op den Camp R, Ivanov S, Hartog M, Limpens E, Jamil M, Smaczniak C, Kaufmann K, et al (2011) Strigolactone biosynthesis in Medicago truncatula and rice requires the symbiotic GRAS-type transcription factors NSP1 and NSP2. Plant Cell **23:** 3853–3865

Morris SE, Turnbull CG, Murfet IC, Beveridge CA (2001) Mutational analysis of branching in pea: evidence that Rms1 and Rms5 regulate the same novel signal. Plant Physiol **126:** 1205–1213

Proust H, Hoffmann B, Xie X, Yoneyama K, Schaefer DG, Yoneyama K, Nogué F, Rameau C (2011) Strigolactones regulate protonema branching

and act as a quorum sensing-like signal in the moss Physcomitrella patens. Development **138:** 1531–1539

Ramakers C, Ruijter JM, Deprez RHL, Moorman AFM (2003) Assumption-free analysis of quantitative real-time polymerase chain reaction (PCR) data. Neurosci Lett **339:** 62–66

Rasmussen A, Mason MG, De Cuyper C, Brewer PB, Herold S, Agusti J, Geelen DNV, Greb T, Goormachtig S, Beeckman T, et al (2012) Strigolactones suppress adventitious rooting in Arabidopsis and pea. Plant Physiol **158:** 1976–1987

Renton M, Hanan J, Ferguson BJ, Beveridge CA (2012) Models of long-distance transport: how is carrier-dependent auxin transport regulated in the stem? New Phytol **194:** 704–715

Ronquist F, Huelsenbeck JP (2003) MrBayes 3: Bayesian phylogenetic inference under mixed models. Bioinformatics **19:** 1572–1574

Ruyter-Spira C, Kohlen W, Charnikhova T, van Zeijl A, van Bezouwen L, de Ruijter N, Cardoso C, Lopez-Raez JA, Matusova R, Bours R, et al (2011) Physiological effects of the synthetic strigolactone analog GR24 on root system architecture in Arabidopsis: another belowground role for strigolactones? Plant Physiol **155:** 721–734

Scaffidi A, Waters MT, Bond CS, Dixon KW, Smith SM, Ghisalberti EL, Flematti GR (2012) Exploring the molecular mechanism of karrikins and strigolactones. Bioorg Med Chem Lett **22:** 3743–3746

Schwartz SH, Qin X, Loewen MC (2004) The biochemical characterization of two carotenoid cleavage enzymes from Arabidopsis indicates that a carotenoid-derived compound inhibits lateral branching. J Biol Chem **279:** 46940–46945

Sorefan K, Booker J, Haurogné K, Goussot M, Bainbridge K, Foo E, Chatfield S, Ward S, Beveridge C, Rameau C, et al (2003) MAX4 and RMS1 are orthologous dioxygenase-like genes that regulate shoot branching in Arabidopsis and pea. Genes Dev **17:** 1469–1474

Stirnberg P, van De Sande K, Leyser HMO (2002) MAX1 and MAX2 control shoot lateral branching in Arabidopsis. Development **129:** 1131–1141

Thirkettle-Watts D, McCabe TC, Clifton R, Moore C, Finnegan PM, Day DA, Whelan J (2003) Analysis of the alternative oxidase promoters from soybean. Plant Physiol **133:** 1158–1169

Umehara M, Hanada A, Magome H, Takeda-Kamiya N, Yamaguchi S (2010) Contribution of strigolactones to the inhibition of tiller bud outgrowth under phosphate deficiency in rice. Plant Cell Physiol **51:** 1118–1126

Umehara M, Hanada A, Yoshida S, Akiyama K, Arite T, Takeda-Kamiya N, Magome H, Kamiya Y, Shirasu K, Yoneyama K, et al (2008) Inhibition of shoot branching by new terpenoid plant hormones. Nature **455:** 195–200

Vallabhaneni R, Bradbury LMT, Wurtzel ET (2010) The carotenoid dioxygenase gene family in maize, sorghum, and rice. Arch Biochem Biophys **504:** 104–111

Waters MT, Nelson DC, Scaffidi A, Flematti GR, Sun YK, Dixon KW, Smith SM (2012) Specialisation within the DWARF14 protein family confers distinct responses to karrikins and strigolactones in Arabidopsis. Development **139:** 1285–1295

Waters MT, Smith SM, Nelson DC (2011) Smoke signals and seed dormancy: where next for MAX2? Plant Signal Behav **6:** 1418–1422

Whelan S, Goldman NA (2001) General empirical model of protein evolution derived from multiple protein families using a maximum-likelihood approach. Mol Bol Evol **18:** 691–699

Xie X, Yoneyama K, Yoneyama K (2010) The strigolactone story. Annu Rev Phytopathol **48:** 93–117

Zhu H, Riely BK, Burns NJ, Ané J-M (2006) Tracing nonlegume orthologs of legume genes required for nodulation and arbuscular mycorrhizal symbioses. Genetics **172:** 2491–2499